Dictating Pt-based Electrocatalyst Performance in Polymer Electrolyte Fuel Cells; from Formulation to Application

Tim Van Cleve.[a] Sunilkumar Khandavalli,[a] Anamika Chowdhury,[b,c] Samantha Medina,[d] Svitlana

Pylypenko,[a,d] Min Wang,[a] Karren L. More,[e] Nancy Kariuki,[f] Deborah J. Myers,[f] Adam Z.

Weber,[b] Scott A. Mauger,[a] Michael Ulsh,[a] and K. C. Neyerlin[a,]*

[a]Chemistry and Nanoscience Center, National Renewable Energy Laboratory, Golden CO, 80401, USA
[b]Energy Conversion Group, Energy Technologies Area, Lawrence Berkeley National
Laboratory, Berkeley CA, 94720, USA
[c]Department of Chemical and Biomolecular Engineering, University of California,
Berkeley CA, 94720, USA
[d]Colorado School of Mines, Golden CO, 80401, USA
[e]Oak Ridge National Laboratory, Oak Ridge TN,
37830, USA [f] Argonne National Laboratory,
Lemont IL, 60439, USA

*Corresponding Author
Email: kenneth.neyerlin@nrel.gov

Effect of Conditioning Protocol on Cell performance

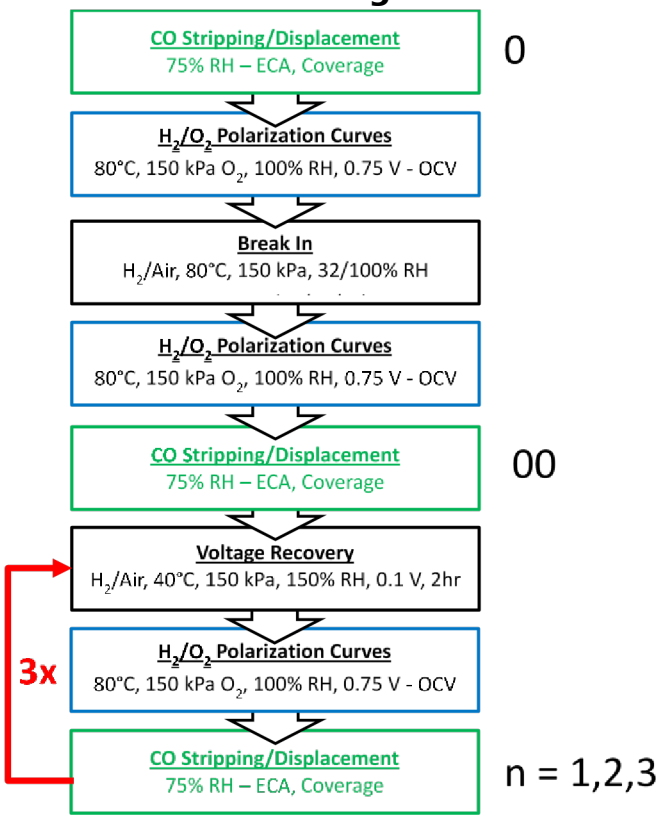

Schema S1. Depiction of CO displacement and testing protocol for 0.1mg cm^{-2} MEAs.

As mentioned in the paper, electrodes were fully conditioned with 3 voltage recovery cycles before characterizing the electrode with an array of *in situ* techniques measuring performance and electrode properties (e.g. ECA, R_{nF}, i_m, i_{sp}, Θ_{SO3-}, etc). In order to compare electrodes at different points during the conditioning protocol, we've developed the following notation. Here 0 and 00 represent characterizing the electrode "as-prepared"/before and after break-in protocol, respectively. 2h voltage recoveries were performed to improve performance and data measured after the i^{th} VR cycle are recorded at point i.

Gas Diffusion Layer (GDL) Compression Calculation

Due to differences in mechanical properties, SGL 29BC and Freudenberg H32C8 GDLs were matched with PFTE gaskets in such a way that GDLs are compressed to 25% and 18% (respectively) their original thickness upon cell assembly (40 in-lb). Equation S1was used to estimate the compression for a pair of gaskets and GDLs with combined thickness of δ2gasket and δ2GDLs, respectively.

$$\text{Compression}\ (\%) = 100\% \times \left[1 - \frac{0.94 \times \delta 2_{\text{GDLs}}}{\delta 2_{\text{gasket}}}\right] \quad [\text{S1}]$$

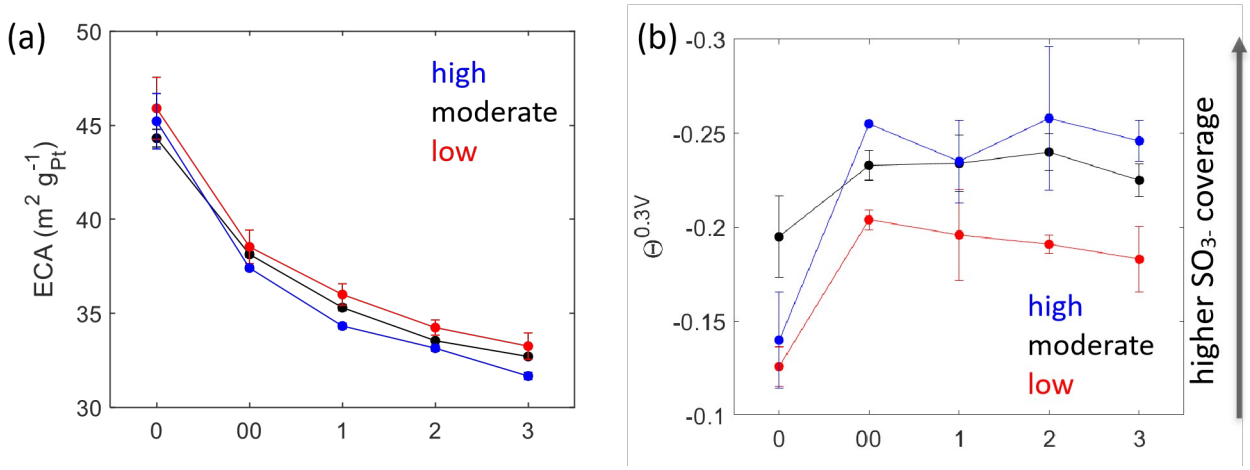

Figure S1. a) Electrochemical surface area (m^2_{Pt} g_{Pt}^{-1}) for 24wt%, 62wt%, and 83wt% MEAs determined from CO stripping voltammetry and XRF as a function electrode conditioning. b) Sulfonate coverage measured by CO displacement at 0.3 V_{cell} as a function of conditioning. Error bars correspond to standard deviation from at least 3 experiments.

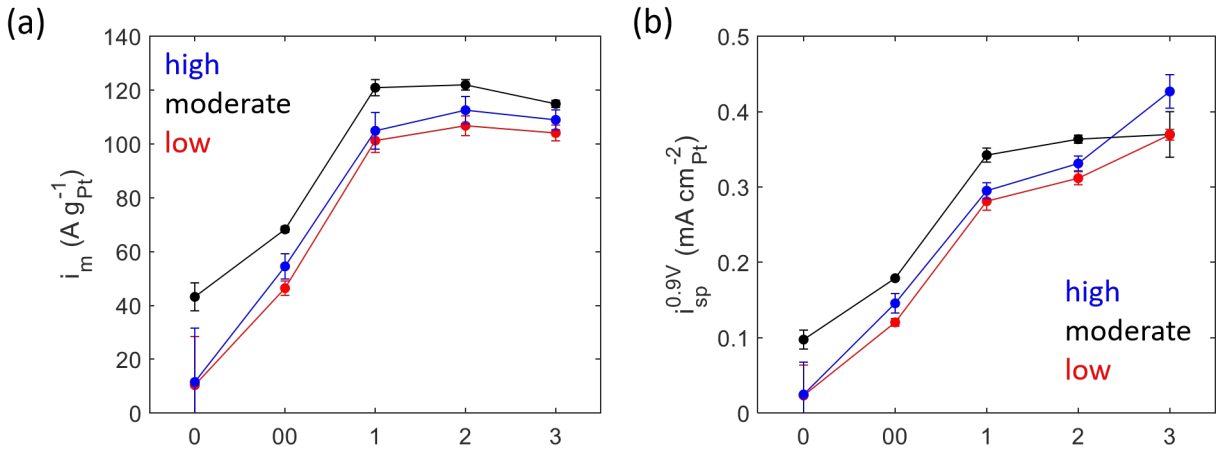

Figure S2. a) Mass and b) specific activities at 0.9 $V_{iR\text{-}free}$ of various 50cm^2 MEA were measured as a function of conditioning and ink formulation. Rates were corrected for H_2 crossover and voltages were corrected for HFR and ionic conductivity resistances. Error bars correspond to the standard deviation from experiments on at least 3 different MEAs.

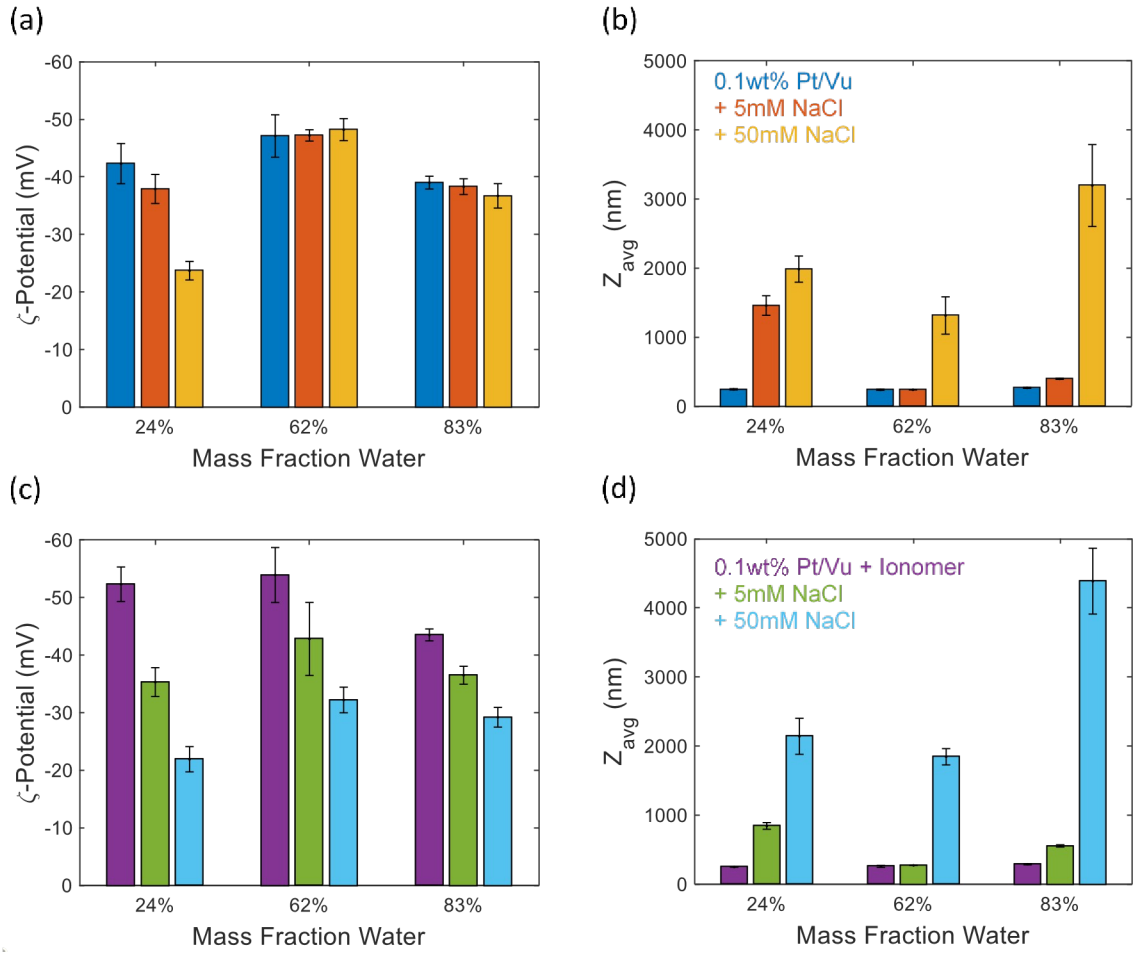

Figure S3. a) ζ-Potential and b) Z_{avg} diameter measurements for 0.1wt% Pt/Vu inks without ionomer and added salt. c) ζ-Potential and d) Z_{avg} diameter measurements for 0.1wt% Pt/Vu inks with ionomer and added salt.

Table S1. pH Measurements of various 0.1wt% Pt/Vu inks.

	pH			
	No ionomer		**With Ionomer**	
H_2O wt %	**0 mM NaCl**	**5 mM NaCl**	**0 mM NaCl**	**5 mM NaCl**
24	5.4	5.9	5.0	6.6
62	4.2	5.5	3.4	5.2
83	3.6	4.9	3.2	4.8

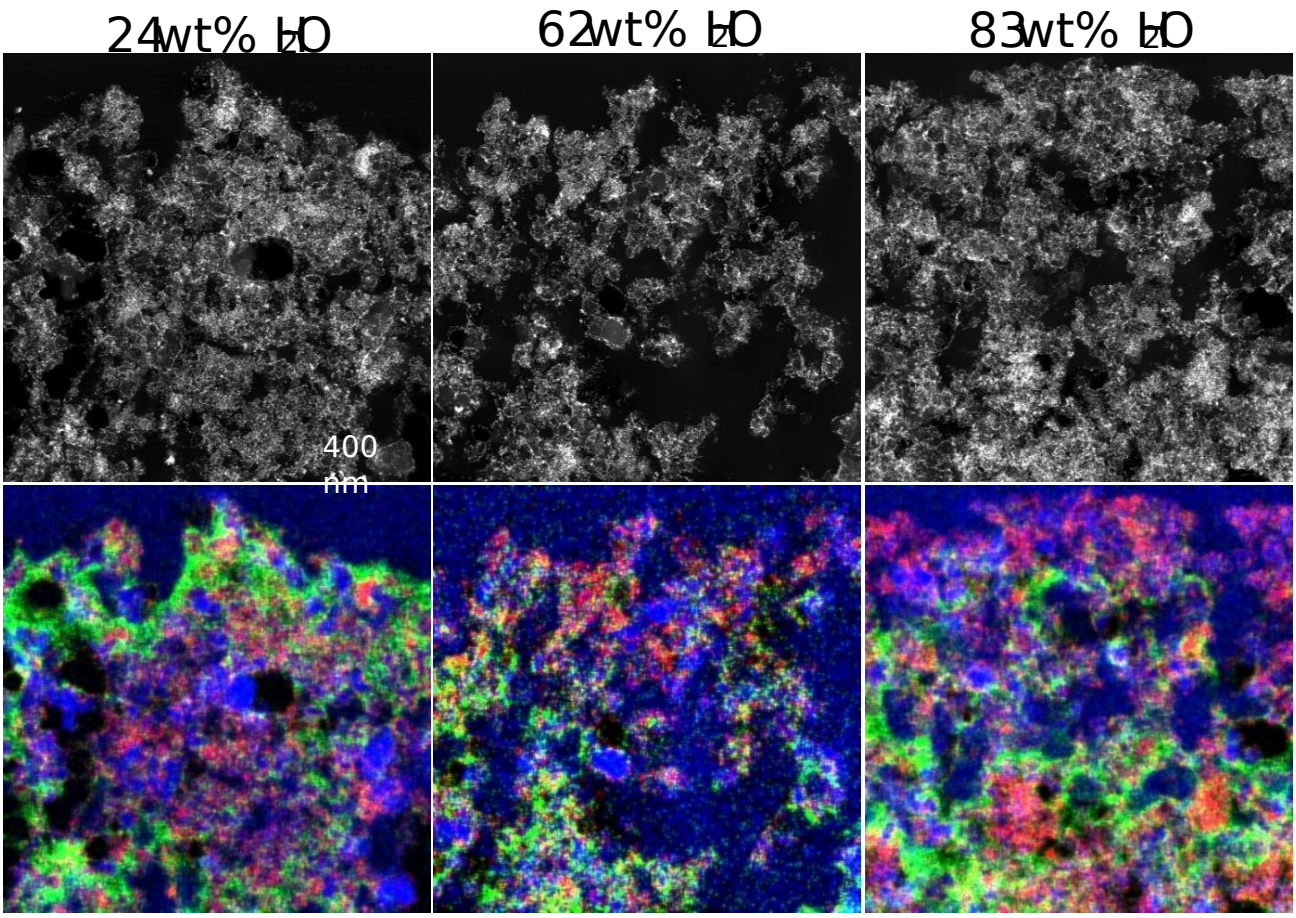

Figure S4. High-magnification elemental maps of Pt (**red**), F (**green**), and C (**blue**) overlayed on corresponding HAADF-STEM-EDS images of MEA cross-sections of 24wt%, 62wt%, and 83wt% catalyst inks.

CO Displacement Chronoamperometry

CO displacement chronoamperometry experiments were performed to measure the coverage of charged species on Pt at different cell potentials. At low potentials ($0.1V_{cell}$), the negatively charge Pt surface adsorbs cationic species like H^+, which exhibit an oxidative current during CO displacement. By increasing the electrode potential, the electrode to become more e^-

deficient (initially less negatively, then more positively charged), leading to anion adsorption on the Pt surface. CO displacement at these higher potentials generates a reductive (negative) current as shown in Figure S5b. Since the interest is in measuring ionomer adsorption, coverages were compared at 0.3V, above the catalyst's potential of zero charge (pzc). Above the pzc, the catalytic surface will have a partial positive charge which will electrostatically attract anionic species such as the sulfonate group of nearby ionomers. In these cases, we assume on the sulfonate group of the ionomer contributes to coverage. At higher potentials, adsorbed CO can immediately oxidize leading to lower Q_{CO} values affecting both ECA and coverage measurements. Displacement charges were determined by integrating the transient reducing current upon the addition of CO as shown in SI Figure S5a. Coverages were determined using the following equation:

$$\theta_{SO_3^+/SO_3^-} = 2 * q_{dis}/Q_e$$

where coverage (Θ) and CO displacement charge (q_{dis}) are potential dependent, and CO stripping charge (Q_e) relates to all accessible Pt sites. Note, there is a stoichiometric constant of 2 because CO oxidization is a $2e^-$ process while CO displacement involves 1 e-. Using this convention, coverages can have a negative charge indicating the adsorption of anionic species when $q_{dis} < 0$.

The largest sulfonate coverages were observed at $0.3V_{cell}$ because this technique is difficult at higher operating potentials (> 0.5V) due to contributions from CO oxidation. Besides, this potential is sufficiently above the *pzc* such the Pt surface is saturated with SO_3^- from nearby ionomer. After the initial MEA break-in step, sulfonate coverages remain constant despite activity improvements following subsequent voltage-recovery cycles (SI Figures S1 and S2). This is an interesting result because it suggests observed benefits in kinetic performance resulting from the break-in and voltage-recovery steps do not relate to changes in the local sulfonate coverage on Pt sites, which remain fixed and are largely determined by ink solvent ratio.

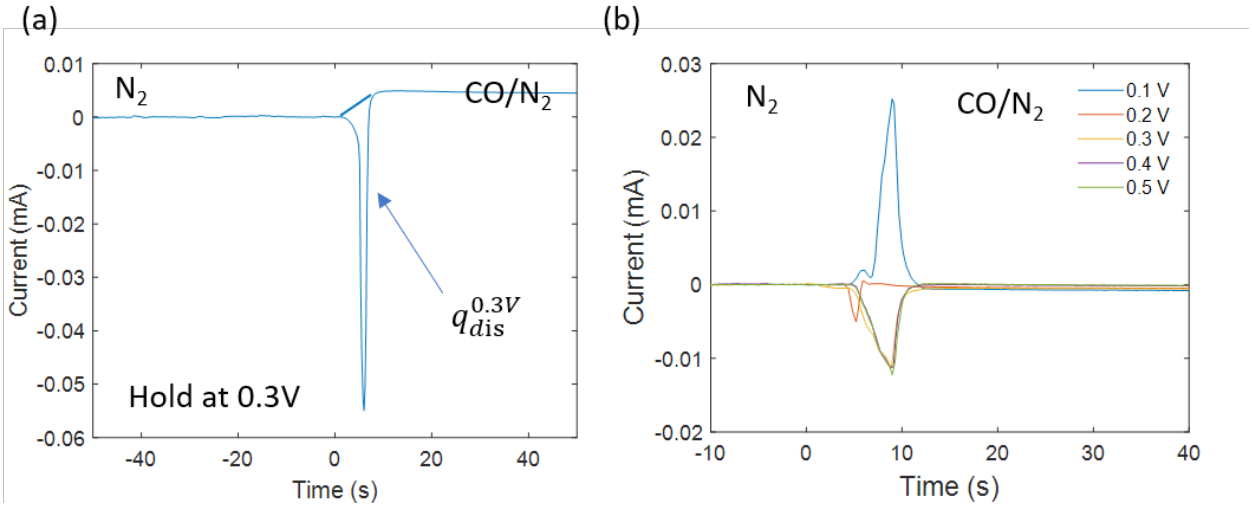

Figure S5. a) Representative CO displacement chronoamperometry spectra taken at $0.3V_{cell}$ indicating linear background used to calculate $q_{dis}^{0.3V}$. b) CO displacement spectra taken at different cell voltages (0.1-0.5V) indicating differences in charged specie coverages.

Ionomer Coverage by EIS

Electrochemical impedance spectroscopy was employed to measure double layer capacitances at wet and dry conditions with and without CO present to estimate CO coverage on Pt and Cu surfaces. Below are Nyquist plots and -1/ ωZ_{im} vs $1/\omega^2$ plots which were used to determine C_{dl} of a single Pt/Vu MEA at different operating conditions. For high loading samples, $-1/\omega Z_{im}$ becomes constant at low ω's (≈ 2 s^2 rad^{-2}) so this value was used to estimate C_{dl} as shown in SI Figure S6.

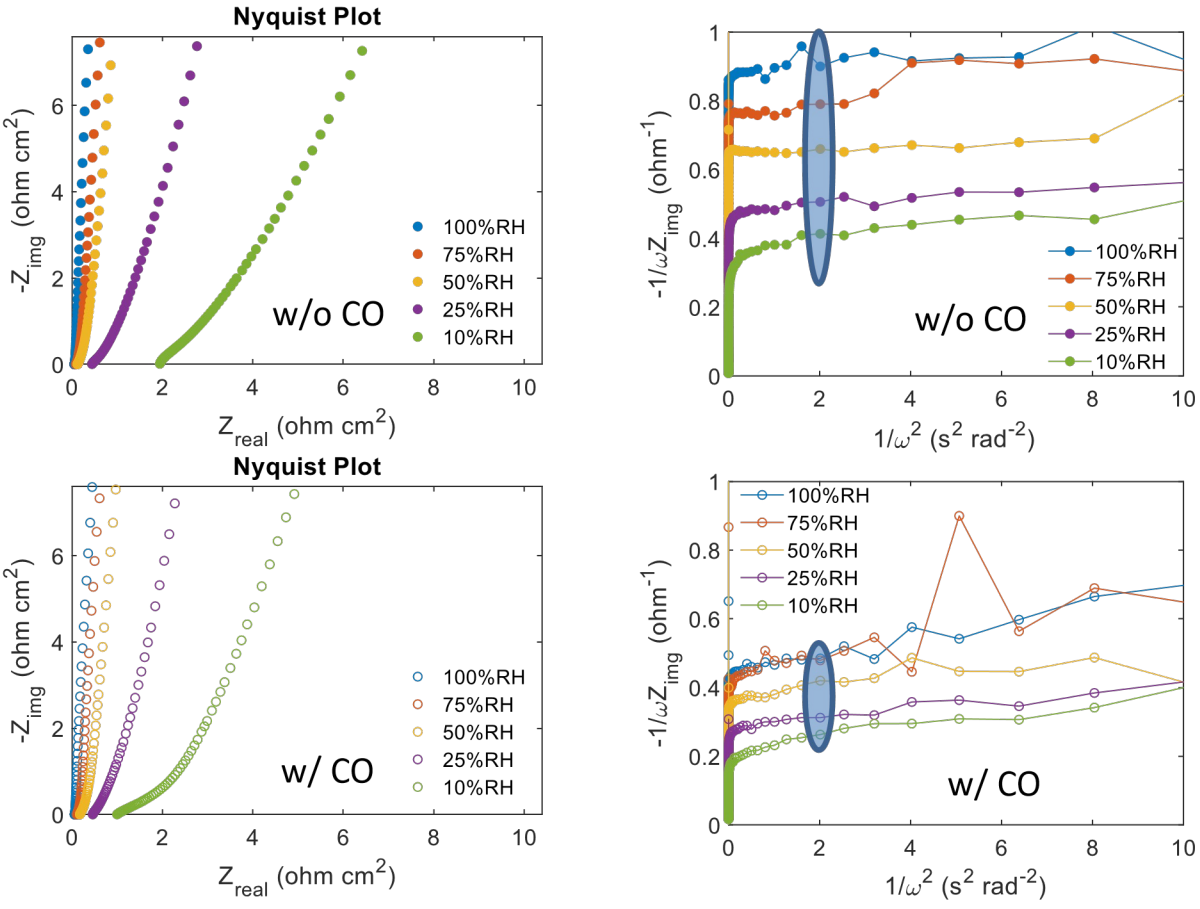

Figure S6. Nyquist and $-1/\omega Z_{img}$ vs $1/\omega^2$ plots on Pt/Vu MEA at 80°C at different relative humidity with and without CO poisoning.

Using the C_{dl} values measured at 10% and 100% RH, with and without CO exposure, it is possible to determine the contributions to total capacitance from C|ionomer, C|water, Pt|ionomer, and Pt|water interfaces, using expressions for C_{dl} (RH, CO) described in Figure 6. Normalizing total capacitance by electrode loading (determined by XRF), it is possible to compare the capacitive contributions of these various interfaces across the Pt/Vu MEA series (Figure S7).

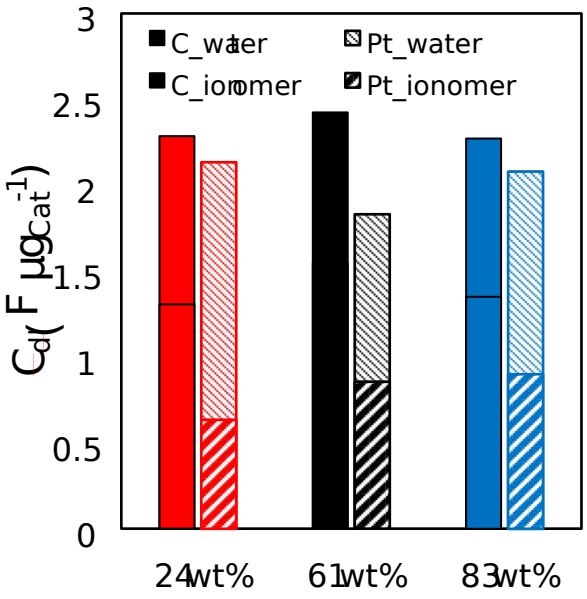

Figure S7. Contributions of Pt and C interfaces contributing to total double layer capacitance on different Pt/Vu MEAs. Error bars correspond to standard deviations from experiments on 3 different MEAs.

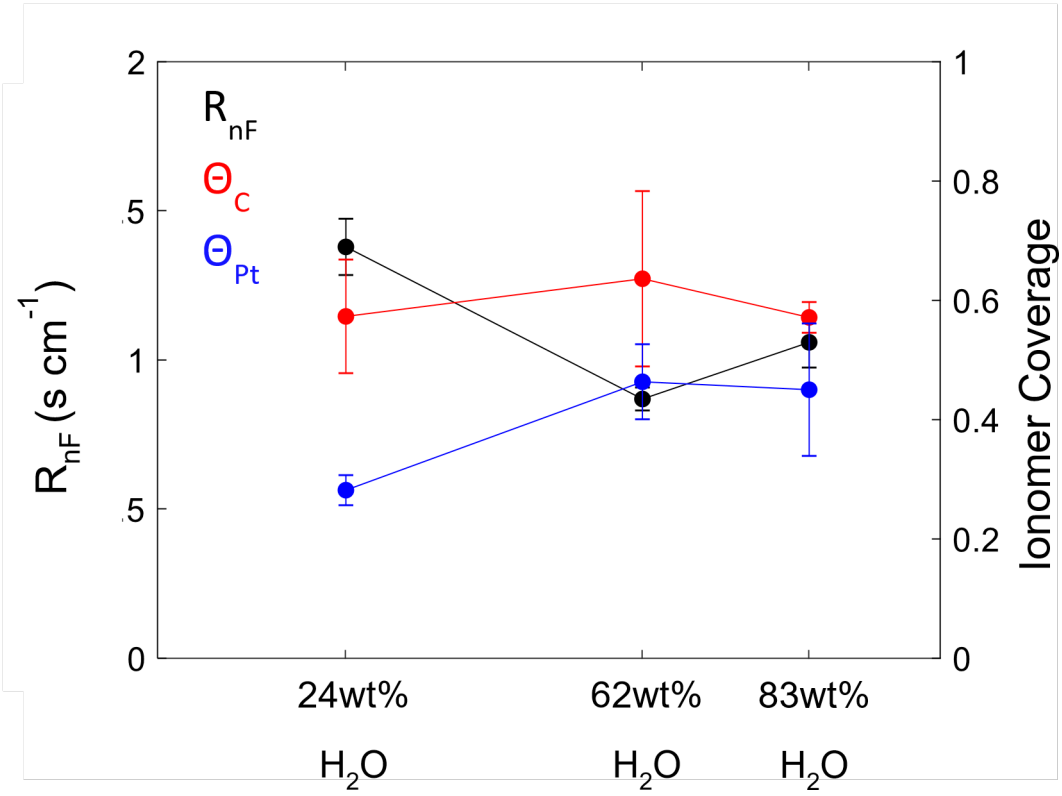

Figure S8. Comparison of non-Fickian transport resistance and ionomer coverages Pt and C measured by EIS as a function of ink solvent ratio.

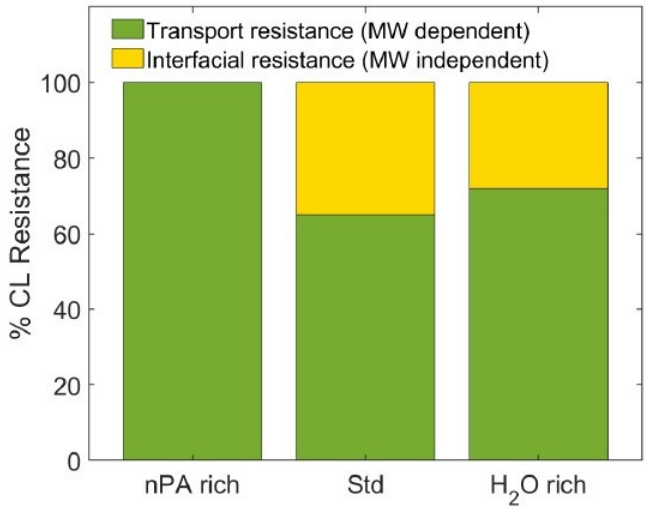

Figure S9. Fractional contribution of interfacial and transport resistance measured by H_2/D_2 limiting current experiments using equation [3].

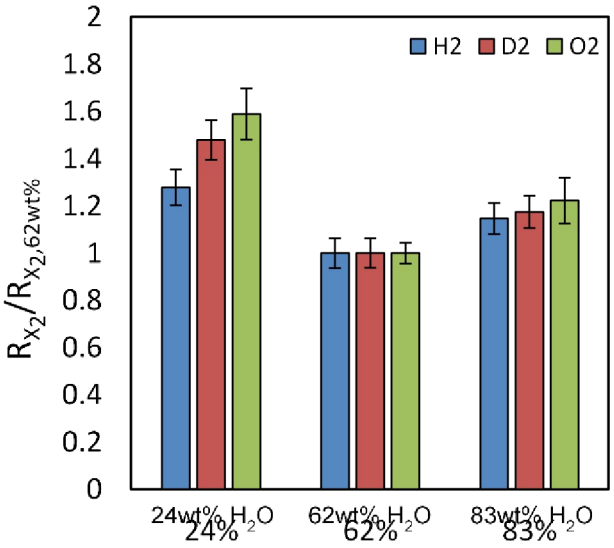

Figure S10. Normalized gas transport resistances ($R_{X2}/R_{X2,62wt\%}$) from various limiting current experiments relative to 62wt% MEAs. Error bars correspond to the standard deviation at least 3 experiments.

Appendix S1: List of Symbols

□(□)	Scattering intensity from USAXS, SAXS experiments
ϱ	Scattering length density of particle
F(q, r)	Scattering function at scattering vector q of a particle of characteristic dimension r
V	Volume of particle with radius r
Np	Number density of particle
□□□□□	Cell voltage
□□□−□□□□	Cell voltage corrected for membrane, electronic, and ionic (H^+) conductivity losses
□	Current density (geometric surface area basis)
□□	Mass activity (current normalized by Pt mass loading determined by XRF)
□□	Specific activity (current normalized by Pt surface area)
□□□	Non-Fickian O_2 transport resistance (P-independent resistance from catalyst layer)
□	Zeta-Potential
□□□□	Average diameter size from DLS experiments

$\theta_{SO_3^-}$	Sulfonate (Anion) coverage measured by CO displacement chronoamperometry
θ_{I}	Ionomer coverage on C measured by AC impedance method
$\theta_{I,Pt}$	Ionomer coverage on Pt measured by AC impedance method
C_{dl}	Total double layer capacitance of electrode measured by AC impedance
$C_{dl,x\|y}$	Double layer capacitance due to specific interface x|y
$R_{gas,film}$	Gas transport resistance from molecular diffusion through ionomer film
f_{int}	Fractional contribution of interfacial resistances